Bridge Deterioration Quantification Protocol Using UAV

Luis Duque, S.M.ASCE[1]; Junwon Seo, Ph.D., P.E., M.ASCE[2]; and James Wacker, M.ASCE[3]

Abstract: This paper focuses on evaluating the effectiveness of an unmanned aerial vehicle (UAV) as a supplementary bridge damage quantification tool. For this study, a glued-laminated timber arch bridge in South Dakota was selected, and an UAV was utilized for the bridge damage quantification. A recommended four-stage UAV-enabled bridge damage quantification protocol involving image quality assessment and image-based damage quantification was developed. A field application using the UAV to measure crack lengths, thicknesses, and rust stain areas of the selected bridge was conducted following the recommended protocol. The image quality parameters, including sharpness and entropy, were used to determine the quality of the UAV-captured images. Pixel- and photogrammetry-based measurements using the high-quality images were obtained to quantify the bridge damage, and the damage was compared to that from actual field measurements. Once the damage information was gathered, the UAV image–based damage level classification was established based on the damage levels defined by current standards. The findings confirmed the accuracy of the recommended protocol, with results within 3.5, 7.9, and 14.9% difference for crack length, thickness, and rust stain area, respectively, when compared with the field measurements. **DOI: 10.1061/(ASCE)BE.1943-5592.0001289.** *© 2018 American Society of Civil Engineers.*

Author keywords: Bridge; Unmanned aerial vehicle (UAV); Image; Pixel; Photogrammetry; Damage; Measurements; Quantification.

Introduction

The use of unmanned aerial vehicles (UAVs) has lately gained interest among structure or bridge inspectors due to costly and inefficient bridge inspection practices currently used. UAVs provide unique capabilities, including the ability to fly near limited-accessibility bridge locations, and carry high-resolution cameras and sensors to overcome current bridge inspection access limitations (Seo et al. 2018b; Guerrero and Bestaoui 2013). In 2013, a study was conducted to estimate the cost required for the inspection of an increasing number of deficient bridges using the current inspection technology with expensive access equipment (Kirk and Mallett 2013). It was reported that the Federal Highway Administration (FHWA) would be required to invest $24.6 billion annually by 2032 to inspect the number of bridges using the current technology. The UAV technology has the potential to efficiently reduce the cost and supplement current bridge inspection procedures to provide safer bridges for future generations.

Different researchers have made significant efforts to detect damage using UAVs (Ellenberg et al. 2016; Hutchinson and Chen 2010; Khaloo et al. 2018; Kim et al. 2015, 2017). For instance, Khaloo et al. (2018) inspected a bridge by developing a three-dimensional (3D) virtual model to observe damage on the bridge. The identified damage included missing bolts, damaged truss connections, and defective truss chords. It was reported that, by conducting the 3D virtual model generation, inspectors were able to observe damage in less time and without risk of injury, as only an UAV was needed to gather all the information. It was also mentioned that the generation of 3D virtual models during the life cycle of the bridge could allow for the analysis of long-term damage, such as camber sag.

Furthermore, Hutchinson and Chen (2010) and Kim et al. (2015) developed innovative alternatives to quantify concrete cracks using UAVs. Kim et al. (2015) developed a crack measurement algorithm known as morphological link for crack (MorphLink-C) to analyze images gathered using an UAV. The algorithm executes a 14-step process to determine the crack area, length, and thickness. The researchers performed a verification test to validate the accuracy of the algorithm. Findings revealed that the proposed algorithm obtained results within 0.08-mm difference when compared to direct measurements.

Most recently, Kim et al. (2017) developed a hybrid image-processing method to obtain crack length and thickness measurements from images captured by an UAV. To complete the measurements, a camera, an ultrasonic displacement sensor, and a wireless fidelity in (WIFI) module were utilized. Then, the implementation of a binarization method (i.e., use of white and black pixels to identify crack boundaries) permitted the estimation of the crack length and thickness. Kim et al. (2017) determined that the method produced accurate results for cracks with thickness greater than 0.1 mm. It was concluded that the maximum percentage error was 7.3% for the crack length, confirming the accuracy of the proposed hybrid method. Although significant findings have been obtained by a number of researchers to quantify damage on bridges, a comprehensive UAV-enabled bridge inspection and damage quantification procedure has not been fully developed to date.

The main objective of this study was to develop an UAV-image-based damage quantification protocol to facilitate both future bridge inspection and damage quantification procedures. This paper is divided into five different sections, including this section. The second section includes a description of the selected UAV and bridge to conduct the study. The third and fourth sections detail the four-stage damage quantification protocol and its application to the

[1]Graduate Student, Civil and Environmental Engineering Dept., South Dakota State Univ., Brookings, SD 57006. Email: luis.duque@sdstate.edu

[2]Assistant Professor, Dept. of Civil and Environmental Engineering, South Dakota State Univ., Brookings, SD 57006 (corresponding author). Email: Junwon.Seo@sdstate.edu

[3]Research Engineer, Forest Service, US Forest Products Lab, One Gifford Pinchot Dr., Madison, WI 53726. Email: jwacker@fs.fed.us

Note. This manuscript was submitted on December 11, 2017; approved on April 18, 2018; published online on August 3, 2018. Discussion period open until January 3, 2019; separate discussions must be submitted for individual papers. This paper is part of the ***Journal of Bridge Engineering***, © ASCE, ISSN 1084-0702.

selected bridge, respectively. Finally, the fifth section presents conclusions drawn from this study and future work.

UAV and Bridge Selection

Prior to beginning the study, an UAV and bridge selection was required. An UAV capable of capturing high-resolution images to determine the damage on the bridge was needed, and a bridge structure, which is suitable for the application of the protocol, was required to perform the damage quantification evaluation. The selection of the UAV and bridge also aimed to provide an affordable UAV-based inspection to county and local governments. Details of the UAV and bridge selection can be seen in the following subsections.

UAV Selection

For the selection of the UAV, a comprehensive comparison between 13 different UAVs from seven different manufacturers was conducted. When selecting the appropriate UAV for the damage quantification, different factors, including flight time, camera location, image resolution, video resolution, payload capacity, UAV lights, remote range, and cost, were considered. Considering these specifications and analyzing the advantages and disadvantages for each UAV, a Dà-Jiāng Innovations (DJI, Shenzhen, Guangdong) Phantom 4 was selected [Figs. 1(a and b)]. The cost-performance ratio provided a high-end UAV with appropriate technology suitable for bridge inspection at an affordable price. In particular, the technology of the DJI Phantom 4 includes the ability to avoid obstacles, with sensors at the front and the bottom; thus, the UAV pilot can be allowed to fly between complicated sections near the bridge. Other relevant specifications, such as the ability to fly without a global positioning system (GPS) signal, high-resolution camera, and 135° camera vertical rotation, allow the UAV to efficiently inspect a bridge. Details on the selection of UAVs can be found in past work by Duque et al. (2018).

Bridge Selection

A bridge located at the junction of Highways 16 and 16A north of Keystone within the Black Hills National Forest in the state of South Dakota was selected for the damage quantification study in conjunction with the UAV [Figs. 2(a and b)]. The selected bridge was the Keystone Wye glued-laminated timber arch bridge, which has three continuous spans at each end-approach and eight continuous spans over the arch. Three glued-laminated timber stringers are spaced at 3.12 m (10.25 ft) on center (o.c.), supporting a reinforced concrete deck having a total width of 7.92 m (26 ft). The bridge has a 49-m (161-ft) arch span length, a total length of 88.4 m (290 ft), and guardrails along the edge of the superstructure.

UAV-Image-Based Bridge Damage Quantification Protocol

To efficiently identify and quantify damage on the bridge using the UAV, a recommended four-stage damage quantification protocol was developed as seen in Fig. 3. It is believed that the protocol is capable of providing a systematic procedure for future-generation bridge damage quantification using UAVs. A description of the recommended protocol stages is presented here.

(a)

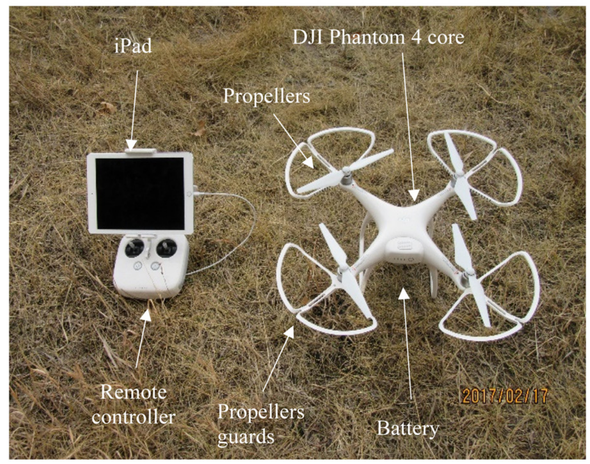

(b)

Fig. 1. DJI Phantom 4: (a) UAV flying near a bridge; and (b) UAV setup prior to inspection. (Images by Junwon Seo.)

In Stage 1, the UAV-enabled bridge inspection is conducted. The inspection of the bridge using the UAV must first consider all safety and regulatory regulations from both the state and federal organizations. For example, state DOT regulations typically do not permit flying UAVs over people, and current Federal Aviation Administration (FAA) airspace restrictions must be followed. It is recommended that the inspection considers the followings: UAV fly operation training, bridge documentation review, bridge surroundings observation, and UAV-preflight check. The skills of the UAV fly operation are needed for the successful bridge inspection. For this study, the researchers (i.e., Duque and Seo) were trained by the certified UAV pilot for a few months to properly and safely operate the UAV. The bridge documentation review is needed for a better understanding of the target bridge configuration and determination of critical sections. The bridge surroundings observation needs to be done to avoid any obstacle to reach the bridge. Some sections of the bridge have tight spaces (e.g., between girders) that the UAV may not able to be close to, resulting in accidental collision. To avoid collision with the bridge, the advanced technology available in the UAV (obstacle avoidance) may be used. For successful UAV fly operation, an UAV preflight check should be done (e.g., check if UAV's and controller's battery are sufficient for the entire bridge inspection). These considerations allow for a safe bridge inspection and efficient flight plan development to identify

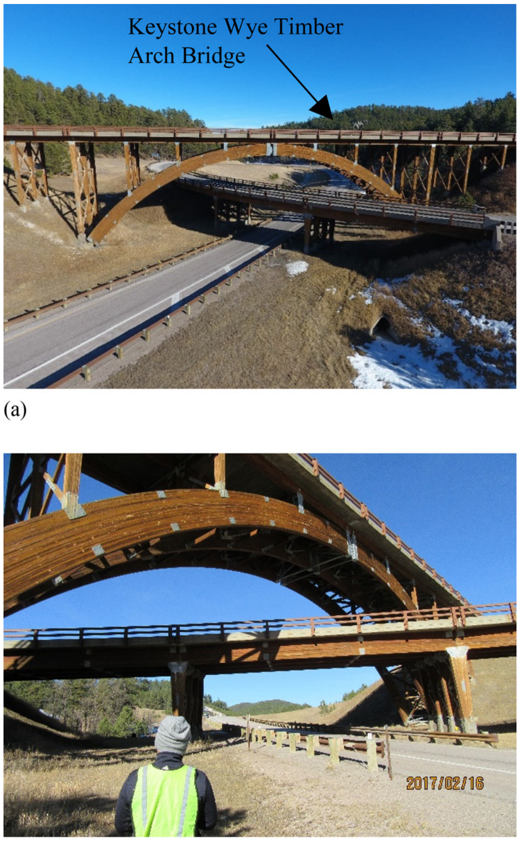

(a)

(b)

Fig. 2. Selected Keystone Wye timber arch bridge: (a) overview of bridge; and (b) view from under the arch. (Images by Luis Duque.)

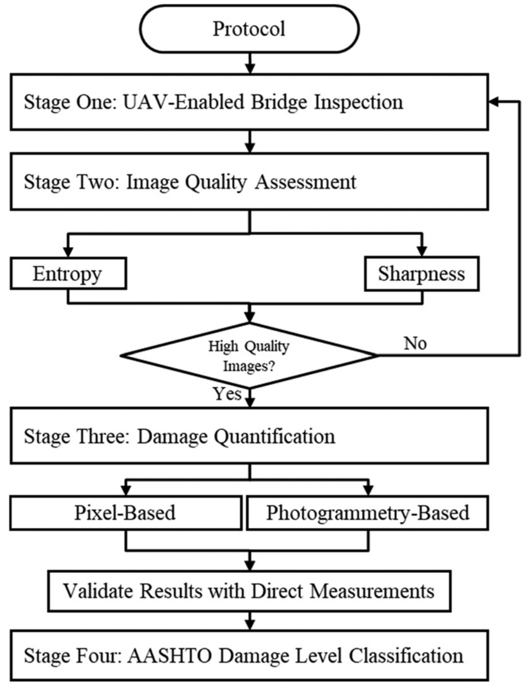

Fig. 3. UAV-image-based bridge damage quantification protocol.

and quantify damage on the bridge. As mentioned, to capture appropriate images, reviewing the bridge documentation (e.g., bridge inspection reports) should be done to determine critical locations. Then, the inspection of the bridge is carried out by gathering overall views and then detailed views of the bridge components.

To efficiently conduct the inspection of the bridge, the images should also be captured following an intended method (i.e., pixel-based or photogrammetry-based methods). If the photogrammetry-based method is to be utilized, images should be captured with at least 60–70% overlap to ensure the 3D virtual model is accurately re-created. More detailed information for the methods used for this study is provided in the next section. During the inspection of the bridge, weather conditions must be considered to avoid unexpected wind gusts while flying near the structure. It is reported that wind speeds of 24.1 km/h (15 mi/h) or higher with wind gusts are unsatisfactory for the operation of the UAV due to instability issues of the UAV (DJI 2018; Seo et al. 2018a, b). Finally, the UAV operator, or pilot-in-command (PIC) who is responsible for operating the UAV, should be continuously assisted by an observer watching the UAV operation at all times via radio communication per FAA regulations.

In Stage 2, the image quality assessment is performed. After the inspection has been completed and all the necessary images are obtained, the image quality assessment can be conducted. During this stage, image quality parameters, including entropy and sharpness, can be implemented to determine the quality of individual images. The two parameters are selected because the use of entropy and sharpness provides a quantifiable value for the visual quality of the image. These parameters are also efficient to determine if an image is blurry or not, which is a common cause of low-quality images. To efficiently identify high-quality images, the values for entropy and sharpness per image are compared to the average value for the entire image set. High-quality images can be identified by: (1) a significant increase in sharpness without a variation in entropy or (2) a significant increase in both parameters due to sufficient illumination.

Benefits of conducting the image quality assessment include the removal of low-quality images not suitable for damage quantification; thus, a reduced number of high-quality images are used for a more efficient damage quantification. It can be noted that once the image quality assessment is completed, the images identified as low-quality should be reviewed to confirm they are unsatisfactory for damage quantification. The low-quality images can be caused by blurriness from adjacent objects, such as moving trees near a bridge due to wind. Finally, a decision considering the number of identified high-quality images should be made. If the number of images gathered is not sufficient for damage quantification, it is recommended that the inspection be repeated to gather higher-quality images for a satisfactory damage quantification.

In Stage 3, the damage quantification is conducted. After all the high-quality images are selected, the damage quantification can be performed. The use of image-analysis software coupled with mathematical algorithms can facilitate the measurement of damage on the bridge. For instance, the use of pixel- and photogrammetry-based methods can be implemented for damage quantification practices. The pixel-based method, which can only use a single image to measure pixels on that image, can be executed utilizing the commercially available image-analysis software, such as ImageJ (Rasband 1997) or PixelRuler (PixelRuler 2018). Visual user interface tools available in these software can allow for efficient damage measurement. To conduct the measurements, a scale must be defined first by the user. The scale is assigned by identifying a known distance on the image (e.g., girder depth). Then, using the line tool, the software determines the number of pixels along the known distance and provides a scale in pixels/cm. The distance unit is defined by the user (i.e., units can also be in meters or millimeters). After the scale is identified, different measurements, such as length and area, can be obtained using the available measuring tool to quantify damage.

In contrast, the photogrammetry-based quantification method uses numerous images to generate a 3D photogrammetric model to quantify damage on the model using software such as PhotoScan (Agisoft PhotoScan 2016) or Drone Deploy (Drone Deploy 2018). The method can utilize the imported georeferenced data from the GPS of the UAV to determine the scale. Once the images are imported, the software identifies unique features from each image and scans the entire image set to align the unique features and produce a sparse point cloud. Then, it creates a dense point cloud and surface to obtain the measurements directly on the model. The surface (also known as mesh) is created using a triangulation method by connecting points in a triangular manner to produce a solid surface. Finally, texture and color corrections are applied based on the information from the imported images to generate a closer representation of the target structure in 3D virtual space. Once the 3D virtual model is completed, the measurements can be conducted using the ruler tool available in the software. Both methods can be validated by comparing the UAV-image-based results to the direct measurements.

In Stage 4, a damage level classification is determined according to the *AASHTO Bridge Element Inspection Guide Manual* (AASHTO 2013). Specifically, during this stage, a damage level classification is assigned in an attempt to provide a quantitative value rather than the descriptive damage states provided by AASHTO. The use of damage quantification methods can be implemented in an attempt to provide an objective structural integrity assessment to minimize inconsistencies in the designation of damage states by bridge inspectors.

Application of Protocol to Keystone Wye Bridge Damage

The following sections include the application of the identified UAV-image-based bridge damage quantification protocol to the selected Keystone Wye Bridge. The findings are presented as follows, subdivided into the aforementioned stages.

Stage 1

To complete an efficient UAV-enabled bridge inspection, the recommended four steps were followed. During the first step, the PIC reviewed the bridge plans and inspection reports provided by the South Dakota DOT (SDDOT). From the bridge plans, the schematic of the Keystone Wye Bridge was plotted as seen in Fig. 4. The component numbering in Fig. 4 was assigned to effectively locate the damage gathered during the UAV-enabled bridge inspection. Moreover, the inspection reports revealed the poor condition of several components, including the abutments and deck, due to severe cracking and water damage. The information from the inspection reports allowed the PIC to identify critical sections for efficient inspection of the bridge.

The second step of Stage 1 was to conduct the observation of the bridge surroundings. During this process, no significant high-risk zones were identified because there were no large trees or structures nearby that may have affected the flight safety. The restrictions from both the SDDOT and FAA were considered prior to takeoff. The SDDOT specified that the operation of the UAV above the bridge deck and highway was prohibited. Furthermore, there were no specific airspace limitations per the FAA regulations because the bridge site was located in Class G airspace, but other regulations pertinent to the operation of the UAV were considered (FAA 2016).

For the third step, the UAV preflight check was conducted. Following both the manufacturer and FAA requirements, the DJI Phantom 4 was inspected thoroughly. Individual components, including rotors, propellers, batteries, iPad, remote controller, gimbal, and software updates, were tested to ensure safety during the flight. The compass was calibrated to guarantee a strong GPS signal prior to flying near the bridge. No issues were found during the preflight check that could have potentially affected the performance of the UAV.

The last step was to conduct the UAV-enabled bridge inspection. During the inspection of the bridge, all regulatory limitations imparted by the SDDOT and FAA were considered. The information gathered from the bridge plans and inspection reports was carefully applied to identify damage on the structure. The deck and other structural components were successfully inspected following the preplanned scheme despite relatively high-wind speeds of 24.1 km/h (15 mi/h). The structural components were inspected by obtaining

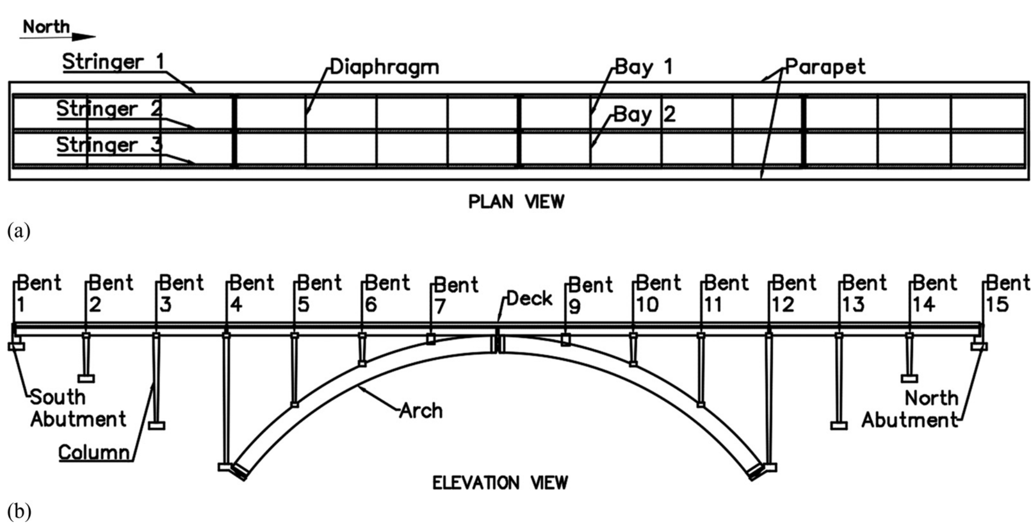

Fig. 4. Keystone Wye Bridge with structural component numbering: (a) component numbering on plan view; and (b) component numbering on elevation view.

overall views first and then proceeding with close-up views of the damage, as seen in Fig. 5. It should be noted that the UAV should be stationary when capturing the images. Fig. 5(a) shows the elevation view of one-half of the bridge, and Fig. 5(b) shows a detailed view of the arch. A sample image of the operation of the UAV can be seen in Fig. 5(c). A complete UAV-enable bridge inspection procedure was provided by Seo et al. (2018a, b).

Stage 2

This section presents a description of the image quality method and its application to the Keystone Wye Bridge.

Image Quality Assessment Method

The image quality assessment method utilized two image quality parameters, including entropy and sharpness, to obtain information on the quality of the images captured from the UAV. In this method, an entropy–sharpness relationship was used to evaluate the quality of individual images. A fictitious image with entropy and sharpness values equal to the average values of the entire set was used as a reference image for the analysis. It is noteworthy that for the efficient damage quantification process, it is important to analyze the high-quality images identified from the proposed method. Details on each image quality parameter and their relationship to determine high-quality images are presented in the following subsections.

Entropy Definition

Entropy can be conventionally defined as the sum of the standard deviation of every color pixel based on a grayscale image. A grayscale 8-bit image has pixel values from 0 (black) to 255 (white) representing the pixel intensity in a grayscale. To provide a single entropy value per image, a mathematical function [as shown in Eq. (1)] available in MATLAB to calculate the entropy of each image was applied (MATLAB 2017). The function measures the sum of pixel intensity from the histogram counts (range of grayscale pixel values) and then determines the standard deviation of intensity from pixel to pixel

$$E = \text{entropy}(I) = -\text{ sum } p. \quad \log 2(p) \tag{1}$$

where E = scalar value of; I = input image in a grayscale; and p = normalized histogram pixel values for grayscale images. A sample image in a grayscale is presented in Fig. 6 with sample grayscale pixel values for a small portion of the image as a visual representation of the input for the entropy function. Fig. 6(a) shows a sample image in a grayscale. Fig. 6(b) shows a small portion of the image with visible pixels, and Fig. 6(c) shows grayscale pixel values corresponding to each pixel within the image.

Sharpness Definition

Sharpness is defined as the transition gradient at pixel intensity boundaries. For instance, if an intensity boundary transitions from white to black, the sharpness value is greater than a transition from white to light gray. To conduct the analysis, a sharpness estimation algorithm developed by Birdal (2011) was implemented. The mathematical process converts the original image into a grayscale to obtain the grayscale pixel boundary gradient. If the transition between pixels was gradual, it was considered blurry, and if that was not the case, it was deemed sharp. A single quantifiable value was obtained by dividing the sum of all the gradient norms (or magnitude of vectors along grayscale pixel boundaries) by the number of pixels on the picture, as seen in Eq. (2)

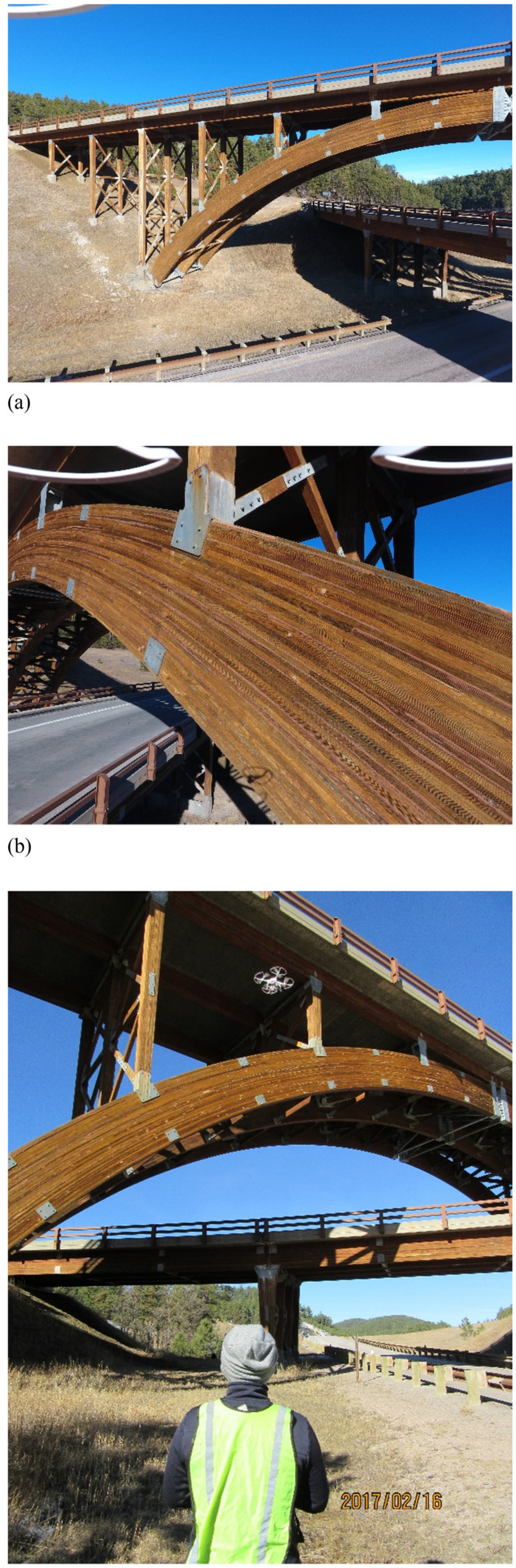

(a) (b) (c)

Fig. 5. Sample images obtained from the inspection of the Keystone Wye Bridge: (a) overall view of the bridge; (b) detailed view of arch; and (c) UAV flying near Keystone Wye Bridge. (Images by Luis Duque.)

(a)

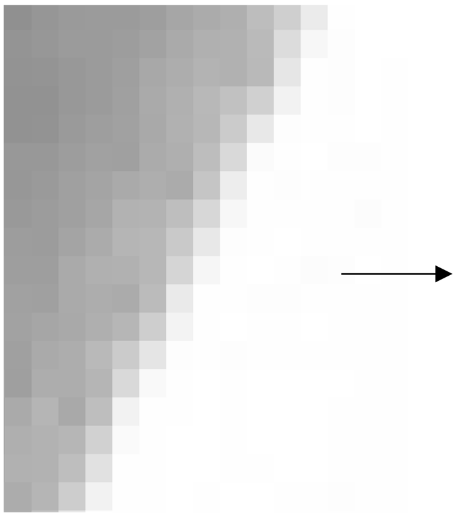

(b)

144	147	151	160	164	168	181	180	220	253	252	255
146	145	156	163	164	175	180	193	227	252	254	255
148	143	156	166	168	186	182	205	244	254	254	255
145	150	162	161	171	187	198	220	253	254	255	255
146	157	163	157	176	186	210	236	253	253	255	255
152	158	160	172	178	191	219	248	252	255	255	255
154	162	162	182	176	200	237	254	251	255	255	255
156	163	162	171	185	214	249	253	254	255	255	255
159	166	172	168	195	226	251	254	255	255	255	255
169	175	175	175	210	239	253	255	255	255	255	255
165	174	176	193	235	251	254	255	255	255	255	255
157	176	178	210	247	254	254	255	255	255	255	255
165	182	180	216	251	254	255	255	255	255	255	255
172	184	194	226	253	255	255	255	255	255	255	255
169	190	220	245	252	255	255	255	255	255	255	255
175	197	231	253	254	255	255	255	255	255	255	255
176	211	243	254	255	255	255	255	255	255	255	255
186	217	253	254	255	255	255	255	255	255	255	255

(c)

Fig. 6. Sample pixel values for an image in grayscale: (a) image in grayscale; (b) small portion of image with visible pixels; and (c) grayscale pixel values for small portion of image.

$$S = \frac{\sum(\sum G)}{P} \quad (2)$$

where S = sharpness; G = gradient vector of pixel in the x- and y-directions; and P = total pixels on the image.

Entropy–Sharpness Relationship

To estimate the quality of the image set obtained from the bridge inspection, a proposed entropy–sharpness relationship was developed. The proposed method calculated both entropy and sharpness along each of the images. Then, the average values for both entropy and sharpness were calculated to establish a fictitious reference image to analyze the captured images in terms of change in sharpness (ΔS) and change in entropy (ΔE). A high-quality image can be determined based upon the variation in the values of the image quality parameters for each image in comparison to the average values in two ways: (1) positive ΔS with negative ΔE, and (2) a positive value for both ΔS and ΔE due to sufficient illumination and good image exposure along with no blurriness. A low-quality image can be identified by a positive ΔE and a negative ΔS due to somewhat low illumination and low image exposure. Finally, a negative value for both ΔS and ΔE requires a visual observation from the inspector to determine if the image has high or low quality.

High-Quality Image Determination

To conduct the image quality assessment, the proposed entropy–sharpness relationship was applied to the 110 images (including different bridge components) gathered during the inspection of the bridge. Specifically, the number of images per component was divided into 25 for the bridge overview, 30 for the arch, 36 for the underside of the deck, 32 for the stringers, 11 for the abutments, and 21 for the columns. It should be noted that more than one component was observed per image. The entropy and sharpness functions were applied to each image to determine their individual values. Then, the average values for the entropy and sharpness were determined to produce a fictitious reference image for comparison. Once all the image quality values per image were gathered, the ΔE and ΔS were determined by comparing the entropy and sharpness of each image to the reference image. A graphical representation of the results obtained can be seen in Fig. 7. In Fig. 7, the top area can be considered the high-quality image region, the bottom-right area shows low-quality images, and the bottom-left section present images that require further review by the inspector to determine the image quality.

Seven sample images are presented in Fig. 7 numbered from 1 to 7 to validate the results obtained. It can be seen that Images 1–3 were high-quality images, as their entropy and sharpness were higher than the reference image, reflected by either a positive ΔS and ΔE or a positive ΔS and a negative ΔE. Images 4 and 5 were identified as low-quality images, as their ΔE was positive and the ΔS was negative. Similarly, Images 6 and 7 were classified as images that require visual assessment by the inspector, as both the ΔS and ΔE were negative when compared to the reference image.

From the sample images presented in the bottom-right area, it is evident that Image 4 was not suitable to identify damage because the arch was underexposed and no damage could be observed. In contrast, Images 6 and 7 would allow the inspector to observe damage on the structure because it was evenly exposed, and all bridge components were clearly visible. The comparison of Images 6 and 7 demonstrated the need to review the images that fall within the bottom-left area. Following this method, a total of 29 images were considered low-quality images not suitable for damage identification;

J. Bridge Eng., 2018, 23(10): 04018080

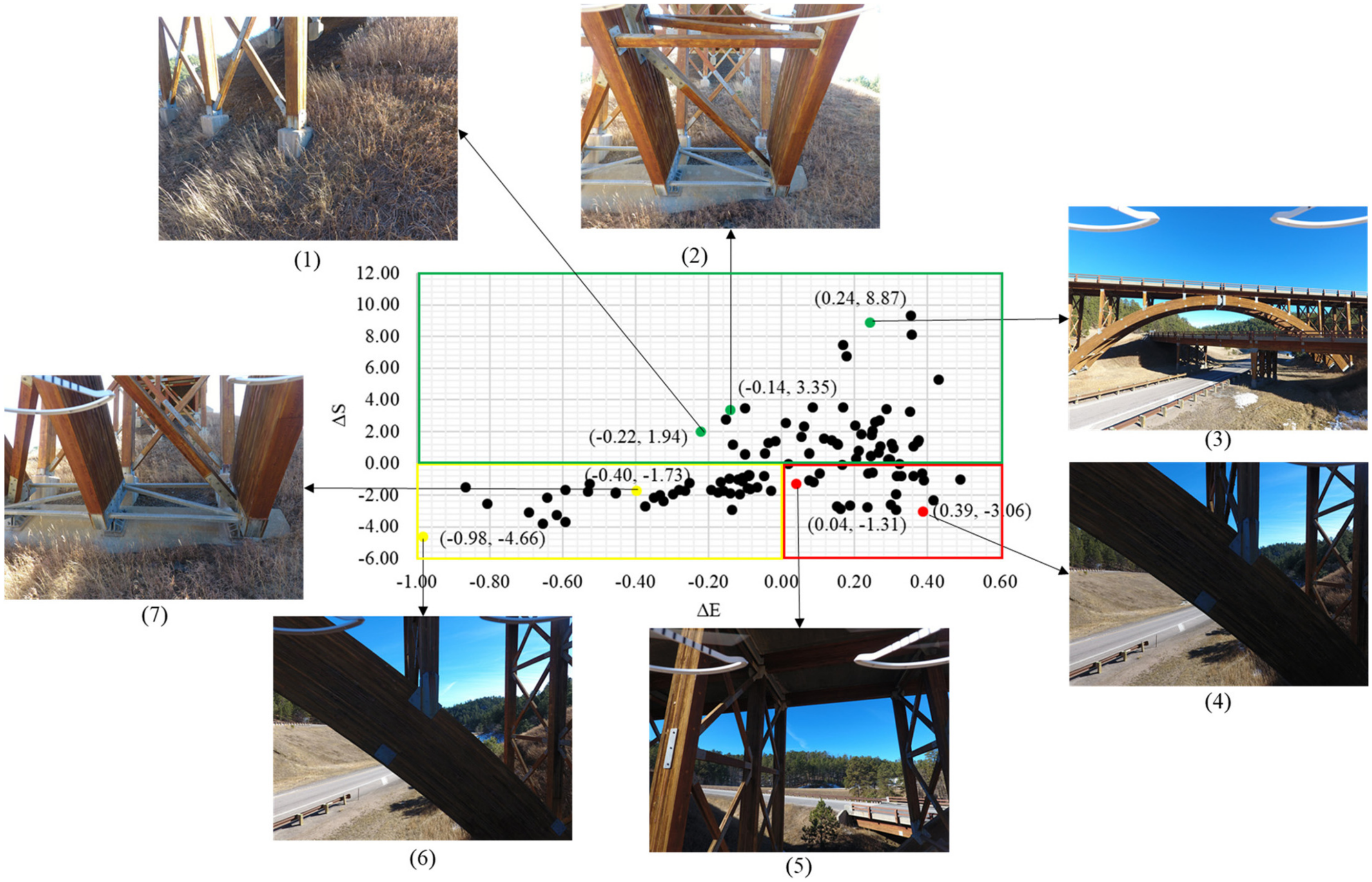

Fig. 7. Graphical representation of entropy–sharpness relationship results with sample images. (Images by Luis Duque, Junwon Seo, and James Wacker.)

therefore, they were removed prior to the damage quantification process. It should be noted that the coverage of 81 images considered high-quality images included the overall bridge section and specific components. It was concluded that the image set presented a sufficient number of high-quality images to conduct the damage quantification in Stage 3.

Stage 3

The selected high-quality images were utilized to conduct the damage quantification. The proposed methods including the pixel- and photogrammetry-based measurements were applied to damage on the bridge to assess their accuracy in more detail. The selected damage was chosen based on physical accessibility to perform the direct measurements, which were compared to those obtained using the UAV. The following subsections present the results of the pixel- and photogrammetry-based measurements in comparison to the field measurements.

Pixel-Based Measurement Results

For the field study of the pixel-based method, a set of two images was gathered from two different angles to evaluate the effect of image distortion on the measurement accuracy. The camera rotation was chosen as one of the recommended camera rotations according to Zhuolei et al. (2009) to produce image distortion. Note that the camera has no capability to calibrate image distortion, but the distortion of the camera lens is negligible. The first image was obtained by taking a picture aligned to the damage at a distance of approximately 1.22 m (4 ft). A graphical represent-ation can be seen in Fig. 8(a), where the solid line represents the field of view for the camera, and the dashed line represents the damage position. For this case, both the field of view and the damage location were aligned; thus, there was not image distortion. A second image to the side of the damage [Fig. 8(b)] was taken at the same distance as in the inspection to capture the first image. This case shows how the solid line representing the field of view for the camera did not match the dashed line showing the damage location; therefore, some image distortion was observed. The study of these two images was considered necessary to evaluate the accuracy of the pixel-based method considering image distortion.

The field study of the pixel-based method was completed by capturing two images from two different angles (i.e., deck image aligned with damage and same image to the side of damage) as seen in Figs. 9(a and b). Using this method, the results specific to a single image were obtained in less than 5 min due to its simple user interface. The time was utilized to define the scale and conduct the needed measurements on the image. To measure the damage, a scale of 22.7 pixels/cm for the image aligned to damage and 28.2 pixels/cm for the image to the side of the damage based upon the depth of the parapet was assigned. It can be noted that the scale must be determined for every image analyzed using ImageJ. The results of the crack length and thickness measurements using ImageJ are presented in Table 1. After completing the measurements of the image aligned to the damage [Fig. 9(a)], the results were compared to the field measurements. The field measurements were completed using a measuring tape. As expected, the results obtained using the pixel-based method were

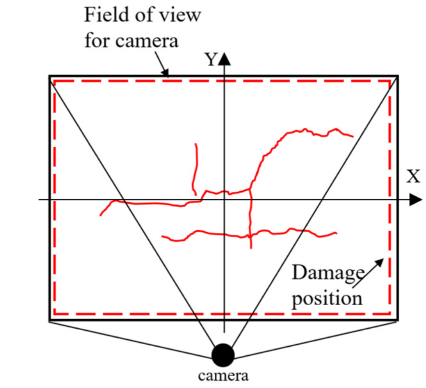

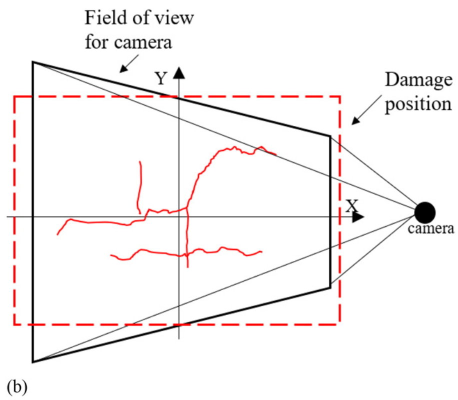

Fig. 8. Image comparison for different camera positions: (a) camera aligned to damage; and (b) camera to the side of damage.

accurate, with percentage difference within 2.7 and 7.9% for the crack length and thickness, respectively.

Contrary to the results for the image aligned to the damage, the analysis for the image taken to the side of the damage presented a percentage difference within 8.7 and 21.9 for the crack lengths and thicknesses, respectively, showing a significant decrease in accuracy. The decrease in accuracy can be attributed to image distortion caused by obtaining the picture to the side of the damage. It was identified that there was an inverse relationship between the accuracy of measurements and the angle between the field of view for the camera and the damage location. The complete set of results for the crack measurements with image distortion are also presented in Table 1.

For the identified rust-stained areas, an approximate area was calculated for the direct measurement. To achieve the measurement, linear segments along the edges of the rust-stained area were directly measured using a measuring tape. Then, using AutoCAD, the simplified irregular shape area was determined. In ImageJ, the available area function was used based on the predetermined scale to calculate the pixel-based area measurements and compare them to field measurements. ImageJ utilizes the scale information and the number of pixels inside the bounded area to complete the measurement. Due to the approximation for the direct measurements, the results were not as accurate as expected, with a percentage difference of 11.9% for the image aligned to the damage, as seen in Fig. 9(c). The study of the rust-stained area on the image to the side of the damage was conducted as seen in Fig. 9(d). As expected, a lower accuracy with a percentage difference of 47.1% when compared to field measurements was observed. The comprehensive results for the study of the rust-stained areas are also included in Table 1.

Photogrammetry-Based Measurement Results

A 3D virtual model based on the aforementioned photogrammetry-based procedure was generated. The 3D virtual model was completed in approximately 40 min (8 times longer than the pixel-based method) using the same computer as the pixel-based method. The computer used to complete the damage quantification had a core i7 processor with 16 GB of random access memory (RAM) and a central processing unit (CPU) of 2.6 Hz. The generation time depended on the size of the 3D virtual model. Furthermore, despite the greater analysis time, the photogrammetry-based method could be beneficial when several damages must be inspected on a bridge section, as only one model would be needed compared to multiple images from the pixel-based method.

In contrast to the analysis of the pixel-based measurements, only one 3D virtual model was developed, as seen in Fig. 10. The model was developed by capturing 20 images with approximately 60–70% overlap as recommended by the software developer. It is worth mentioning that the image distortion determined during the pixel-based method was introduced by an attempt to capture a 3D object using a two-dimensional (2D) image. For that reason, the measurements using the photogrammetry-based method did not present any image distortion because they were conducted directly on the 3D virtual model.

To conduct the measurements, a scale to georeference the 3D virtual model was defined. To establish the scale, the GPS location information from the UAV was utilized, in addition to the assignment of known distances on the 3D virtual model. Then, using the ruler tool, the measurements for the same crack lengths and thicknesses were obtained and compared to the field measurements. The results demonstrated the level of accuracy the method was able to obtain, with percentage differences within 3.5 and 7.4% for the crack lengths and thicknesses, respectively. The details of the results for the crack measurements can be seen in Table 2.

For the rust-stained area measurements, the desired area was isolated from the rest of the 3D virtual model, as seen in Fig. 10. Then, using the *area and volume* function available in PhotoScan, the measurement was completed. PhotoScan estimates the area of the isolated portion of the 3D virtual model by calculating the sum of individual areas for the triangles created to produce the surface of the 3D virtual model. The results were within an acceptable range, with a difference of 14.9% considering the field measurements were approximated. A summary of the results for the rust-stained area measurements is also included in Table 2.

Stage 4

The final stage of the proposed UAV-image-based bridge damage quantification protocol was to establish the damage level following the *AASHTO Bridge Element Inspection Guide Manual*, as seen in Table 3 (AASHTO 2013). A summary of the identified damage level per damage is presented in Table 4. The damage was assigned following both the pixel- and photogrammetry-based results. It was determined that the results between the pixel- and photogrammetry-based methods presented an acceptable percentage difference of less than 4%; therefore, the damage level following the AASHTO manual was assigned based on the average value of the results as shown in Table 4. It is worth mentioning that the AASHTO manual does not include a quantifiable value for the rust-stained areas, but rather a descriptive damage state is presented. Therefore, the damage level was assigned based on the image data (see Fig. 9 and quantified value). A specific damage level for the crack length is not included in the AASHTO manual. It is worthwhile to note that the damage would be subjective due to the lack of quantifiable values in AASHTO.

J. Bridge Eng., 2018, 23(10): 04018080

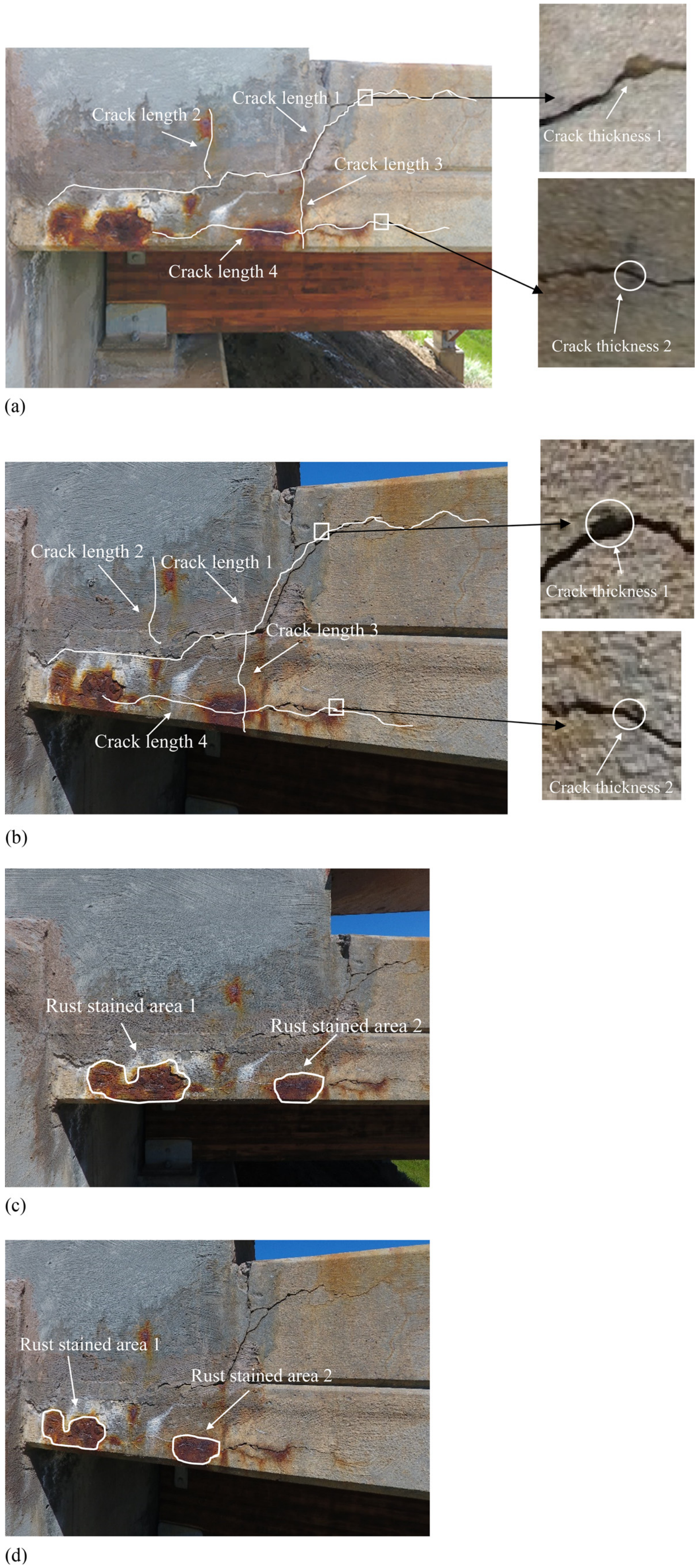

Fig. 9. Pixel-based damage quantification of damage near abutment of the Keystone Wye Bridge: (a) image aligned with damage; (b) image to the side of damage; (c) identified rust-stained areas for image aligned to damage; and (d) identified rust-stained areas for the image to the side of damage.

Table 1. Results from measurements obtained using ImageJ

Damage type	Identified damage	Pixel-based measurement		Field measurement	Measurement difference (%)	
		Aligned to damage	To side of damage		Aligned to damage	To side of damage
Crack length [cm (in.)]	1	127.3 (50.1)	121.7 (47.9)	126.4 (49.75)	0.7	3.8
	2	18.8 (7.4)	17.3 (6.8)	18.3 (7.2)	2.7	5.6
	3	20.2 (7.97)	20.1 (7.9)	20.3 (8 in)	0.5	1.0
	4	82.8 (33)	75.7 (29.8)	82.6 (32.5)	0.2	8.7
Crack thickness [cm (in.)]	1	0.66 (0.26)	0.76 (0.3)	0.61 (0.24)	7.9	21.9
	2	0.14 (0.054)	0.15 (0.06)	0.13 (0.051)	7.4	14.3
Rust-stained area [cm^2 ($in.^2$)]	1	226.5 (35.1)	156.1 (24.2)	252.3 (39.1)	10.8	47.1
	2	91.0 (14.1)	67.7 (10.5)	102.6 (15.9)	11.9	40.1

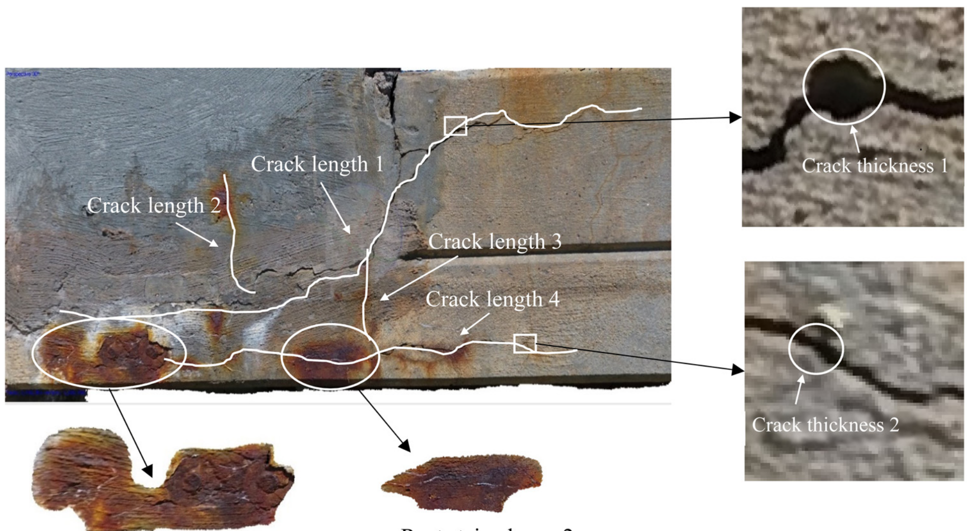

Fig. 10. Photogrammetry-based 3D virtual model for damage quantification of damage near abutment of Keystone Wye Bridge.

Table 2. Results from measurements obtained using PhotoScan

Damage type	Identified damage	Photogrammetry-based measurement	Field measurement	Measurement difference (%)
Crack length [cm (in.)]	1	126.0 (49.6)	126.4 (49.8)	0.3
	2	18.8 (7.4)	18.3 (7.2)	2.7
	3	19.6 (7.7)	20.3 (8.0)	3.5
	4	80.2 (31.2)	82.6 (32.5)	2.9
Crack thickness [cm (in.)]	1	0.64 (0.25)	0.61 (0.24)	4.8
	2	0.14 (0.055)	0.13 (0.051)	7.4
Rust-stained area [cm^2 ($in.^2$)]	1	228.4 (35.4)	252.3 (39.1)	9.9
	2	88.4 (13.7)	102.6 (15.9)	14.9

Table 3. Damage level classification adopted from the AASHTO (2013)

Defects	Condition states			
	1 (Good)	2 (Fair)	3 (Poor)	4 (Severe)
Efflorescence/ rusting staining	None	Surface white without buildup or leaching without rust staining	Heavy buildup with rust staining	The condition warrants a structural review to determine the effect on strength or serviceability of the element or bridge; or a structural review has been completed and the defects impact strength or serviceability of the element or bridge
Cracking (RC and others)	Insignificant cracks or moderate-width cracks that have been sealed	Unsealed moderate-width cracks or unsealed moderate pattern (map) cracking; cracks from 0.03 cm (0.012 in.) to 0.13 cm (0.05 in.) wide	Wide cracks or heavy pattern (map) cracking; cracks greater than 0.13 cm (0.05 in.) wide	

Source: Data from AASHTO (2013).

Table 4. Summary of results for quantification methods and damage level classification

Damage type	Identified damage	Photogrammetry-based measurement	Pixel-based measurement aligned to damage	Measurement difference (%)	Average value	AASHTO damage level
Crack length [cm (in.)]	1	126.0 (49.6)	127.3 (50.1)	1.03	126.65 (49.8)	—
	2	18.8 (7.4)	18.8 (7.4)	0	18.8 (7.4)	—
	3	19.6 (7.7)	20.2 (7.97)	3.02	19.9 (7.8)	—
	4	80.2 (31.6)	82.8 (32.6)	3.4	81.5 (32.1)	—
Crack thickness [cm (in.)]	1	0.64 (0.25)	0.66 (0.26)	3.1	0.65 (0.26)	Poor or more
	2	0.14 (0.055)	0.14 (0.054)	0	0.14 (0.1)	Poor
Rust-stained area [cm^2 ($in.^2$)]	1	228.4 (35.4)	226.5 (35.1)	0.84	227.45 (35.3)	Poor
	2	88.4 (13.7)	91.0 (14.1)	2.9	89.7 (13.9)	Poor

Conclusions

This study aimed to propose an UAV-image-based damage quantification protocol to facilitate bridge inspection and structural integrity evaluation procedures for future generations. The study was completed by executing the proposed protocol to quantify the damage on the Keystone Wye Bridge. Based on the results observed, the following conclusions were made:

1. The UAV operation presented some limitations caused mainly by unfavorable weather conditions, including wind speed, limited illumination, and image over- and underexposure. During the UAV-based inspection, it was difficult to capture damage in regions that were not properly illuminated and operate the drone to reach the bridge under severe wind conditions. However, the UAV was able to capture sufficient high-quality imagery for the damage quantification process by operating under clear weather conditions, gathering sufficient images from different angles of the camera, and performing the image quality assessment.
2. The proposed entropy-sharpness-based image quality assessment method enabled an efficient selection of high-quality imagery to be used in the damage quantification process. The use of a fictitious reference image to determine the variation of the entropy and sharpness per image allowed for an effective detection of unsatisfactory images. During this process, a total of 81 out of 110 images were identified as high-quality images based upon the proposed entropy–sharpness relationship.
3. The pixel-based method that was applied to the damage near the bridge abutment was efficient to obtain measurements, as the results were obtained within 5 min from a single image. The accuracy of the method was reflected in the results for the image aligned to the damage, with results within 12% when compared to the direct measurements. It is noteworthy that the one image aligned with damage and the other image to the side of damage were only considered for the accuracy investigation. Some of the disadvantages of these methods included the inability to obtain accurate results when the camera was not aligned to the damage, as shown in the results for the image to the side of the damage.
4. The photogrammetry-based method that was also applied to the damage selected for the pixel-based method's accuracy investigation was accurate when conducting the crack length, thickness, and rust-stained area measurements, with results falling within 3.5, 7.4, and 14.9% difference, respectively, when compared to direct measurements. A drawback of this method is the amount of time it takes for the computer software to generate the 3D virtual model. For the accurate 3D virtual model recreated in this study, the generation time was approximately 40 min because this method required several images with at least 60–70% overlap, approximately 8 times longer when compared to the pixel-based method, which only required an image aligned to the damage.
5. The use of quantifiable values could provide a more systematic and straightforward determination of the damage level if they are integrated within the AASHTO manual. It is hoped that measurable values for the damage state could allow for a rational structural integrity assessment of the bridge. Finally, it is expected that the quantifiable values for the damage level classification will minimize the discrepancies for the damage level designation by inspectors.

It is recommended that future research be conducted to verify the efficiency of the proposed UAV-image-based method in terms of time, expenses, and safety risk reduction. The study of other bridge types, including concrete and steel, should be conducted to verify the applicability of the recommended damage quantification protocol. The pixel- and photogrammetry-based methods were accurate when compared to field measurements. However, more efficient photogrammetry-based methods in terms of 3D virtual model generation time should be investigated. In contrast, effective methods to minimize the effect of distortion should be further studied for more accurate pixel-based measurements when the images having damage are taken from different side views. A further study to conduct 3D bridge-scanning measurements using UAV equipped with LIght Detection and Ranging (LiDAR) sensors should also be explored.

Acknowledgments

Financial support for this research was provided by the FHWA through the Forest Products Laboratory (USDA-Forest Service). The assistance and cooperation of the SDDOT is gratefully acknowledged.

References

AASHTO. 2013. *AASHTO bridge element inspection guide manual.* Washington, DC: AASHTO.

Agisoft PhotoScan. 2016. "Professional ed." St. Petersburg, Russia: Agisoft LLC.

Birdal, T. 2011. "Sharpness estimation from image gradients." *MathWorks File Exchange*. Natick, Massachusetts: The MathWorks, Inc.

DJI. 2018. "DJI Phantom 4." Accessed March 6, 2018. http://www.dji.com/product/phantom-4/info#specs.

Drone Deploy. 2018. "Field scanner." Drone Deploy. Accessed January 30, 2018. https://www.dronedeploy.com/fieldscanner.html.

Duque, L., J. Seo, and J. Wacker. 2018. "Synthesis of unmanned aerial vehicle applications for infrastructures." *J. Perform. Constr. Facil.* 32 (4): 04018046. https://doi.org/10.1061/(ASCE)CF.1943-5509.0001185.

Ellenberg, A., A. Kontsos, F. Moon, and I. Bartoli. 2016. "Bridge related damage quantification using unmanned aerial vehicle imagery." *Struct.*

Control Health Monit. 23 (9): 1168–1179. https://doi.org/10.1002/stc.1831.
FAA (Federal Aviation Administration). 2016. *Code of federal regulations (14 CFR) part 107.* Washington, DC: FAA.
Guerrero, J. A., and Y. Bestaoui. 2013. "UAV path planning for structure inspection in windy environments." *J. Intell. Robotic Syst.* 69 (1–4): 297–311. https://doi.org/10.1007/s10846-012-9778-2.
Hutchinson, T. C., and Z. Chen. 2010. "Image-based framework for concrete surface crack monitoring and quantification." *Adv. Civ. Eng.* 2010: 1–18. https://doi.org/10.1155/2010/215295.
Khaloo, A., D. Lattanzi, K. Cunningham, R. Dell'Andrea, and M. Riley. 2018. "Unmanned aerial vehicle inspection of the Placer River Trail Bridge through image-based 3D modelling." *Struct. Infrastruct. Eng.* 14 (1): 124–136. https://doi.org/10.1080/15732479.2017.1330891.
Kim, H., J. Lee, E. Ahn, S. Cho, M. Shin, and S.-H. Sim. 2017. "Concrete crack identification using a UAV incorporating hybrid image processing." *Sensors* 17 (9): 2052. https://doi.org/10.3390/s17092052.
Kim, J., S. Kim, J. Park, and J. Nam. 2015. "Development of crack detection system with unmanned aerial vehicles and digital image processing." *Advances in Structure Engineering and Mechanics.* Incheon, Korea: International Associate Structural Engineering and Mechanics (IASEM).
Kirk, R. S., and W. J. Mallett. 2013. *Highway bridge conditions: Issues for congress.* CRS Rep.7-5700. Washington, DC: Congressional Research Service.
MATLAB. 2017. "Entropy." MathWorks documentation. Accessed October 18, 2017. https://www.mathworks.com/help/images/ref/entropy.html.
PixelRuler. 2018. "Pixel ruler." Mioplanet. Accessed January 30, 2018. http://download.cnet.com/Pixel-Ruler/3000-12565_4-75312528.html.
Rasband, W. 1997. "ImageJ." Bethesda, MD: National Institute of Health.
Seo, J., L. Duque, and J. Wacker. 2018a. "Drone-enabled bridge inspection methodology and application." *Automation in Construction* 94: 112–126.
Seo, J., J. Wacker, and L. Duque. 2018b. "Evaluation of unmanned aircraft systems as a bridge inspection tool." Madison, WI: U.S. Dept. of Agriculture, Forest Service, Forest Products Laboratory. Forthcoming.
Zhuolei, W., X. Yanli, L. Yingcheng, Z. Lijian, and Z. Lina. 2009. "Analyse on image distortion caused by camera tilting angle in mosaic camera." In *Proc., Int. Conf. on Geo-spatial Solutions for Emergency Management and the 50th Anniversary of the Chinese Academy of Surveying and Mapping*. Beijing: International Society Photogrammetry and Remote Sensing (ISPRS).